International Journal of
INTELLIGENT SYSTEMS AND APPLICATIONS IN ENGINEERING
ISSN:2147-6799 www.ijisae.org Original Research Paper

Load Frequency Control of Modern Interconnected Power System Using SCSO-SNN Approach

V. Devaraj, M. Kumaresan

Submitted: 22/03/2023 **Revised**: 24/05/2023 **Accepted**: 11/06/2023

Abstract: The operation and design of modern interconnected power systems rely heavily on load frequency regulation. The integration of wind power, photovoltaic energy, and other new energy sources into the power grid has presented significant challenges to the power system. The objective of this work is maximizing the energy output, efficiency and reduced the error of the wind and solar energy system. The less efficient and older power plants are not operated continuously and are only used during peak hours. As a result, an integrated system can help power plants run more efficiently. Also, in wind power fluctuation adds negatively to power imbalance and frequency deviation. To overcome this Problem, we proposed hybrid method is the combined with Sand Cat Swarm Optimization (SCSO), and Spiking Neural Network (SNN). The SCSO generate the control signal of the converter and the SNN method predicts the control signal from the SCSO method. By then, the SCSO-SNN technique is performed in MATLAB platform and the implementation is calculated with the present procedures. The proposed method shows better results in all approaches like, Particle Swarm Optimization (PSO), Ant Lion Optimization (ALO) and Sand Cat Swarm Optimization (SCSO). The proposed method SCSO-SNN compared with existing methods error of battery, Photovoltaic, wind with battery error value is 2.7%.

Keywords: *Photovoltaic system, Wind Turbine, Hybrid, Load frequency, Power plant, Converter, PID controller and solar field.*

1. Introduction

Transmission lines link the contemporary power system network to several regulated locations [1]. The most important factor in determining how efficiently, steadily, and reliably linked power systems operate is the regulation of active power and frequency [2]. The power system unit is continually at risk from changing loading conditions in real life, which might cause the equilibrium states of power system operation to be disrupted. Any abrupt change in frequency results in the instability of power systems since the term frequency and active power are intimately associated [3]. Electric motors, transformers, and other devices may lose synchronization and produce excessive magnetizing current in the event of a significant shift in frequency [4]. Consequently, in order to maintain frequency stability and synchronization with surrounding places, Modern power systems incorporate the load-frequency controller (LFC) with a governor control mechanism. The LFC function, a supervisory controller function, aims to maintain system frequency within a constrained area by attempting to match the generation trend with rising load demand. Likewise, switch tie-line electricity at the appropriate times [5]. In a contemporary power system, LFC is a key auxiliary function that supports power exchanges while simultaneously improving market conditions for energy [6]. Controlling active and reactive power is necessary for preserving the steady-state of system. The goal of the control strategy in an interrelated scheme is to create and distribute electricity as inexpensively as possible and consistently as feasible while keeping the frequency as well as voltage within suitable limits [7].

It is important to remember that a phenomena known as the Load Frequency Control method controls the frequency and active power. With the latest growth of massive interrelated systems, this notion has additional received study attention and made the functioning of the linked system more practical [8]. In addition, a contemporary huge linked network makes it impossible to physically regulate power generation to balance the power demand. Therefore, each generator has equipment placed for automated generation and voltage management. Additionally, the controller is set up for a particular working situation and often handles any little changes in load demand without exceeding the permitted limits for voltage and frequency [9]. LQR controllers have recently received a lot of attention and research interest. Similar to this, interest in the LQR controller is growing. To improve dynamic response and remove or reduce steady-state faults, AGC and LFC frequently employ the widely used classical integer-order proportional-integral controller and proportional integral derivative controller [10]. The LQR problem, a quadratic function, establishes the cost function and a set of linear differential equations explains

[1]*Department of Electrical and Electronics Engineering, Dr. M.G.R Educational and Research Institute, Chennai, Tamil Nadu 600095 India. Email:djran14@gmail.com*
[2]*Department of Electronics and Communication Engineering, Dr. M.G.R Educational and Research Institute, Chennai, Tamil Nadu 600095 India*

the dynamics of the system. The LQR offers the best answer, according to one of the key theoretical discoveries [11]. Numerous researches have been done so far on the load frequency control strategy of linked power systems. In a multi-area power system, a hybrid approach is utilized to develop a fuzzy PI/PID controller for load frequency control [12]. The research employs the evolutionary method to create the fuzzy PI/PID-controllers' scaling factors for a 2 region thermal-power system. [13]. In this regard, the method's viability is determined using a range of system characteristics and loading scenarios. Additionally, a fuzzy PI/PID controller for the AGC of conventional/restructured multi-area linked power-systems is in [14] and is depends on a bacterial foraging optimization algorithm. The findings of simulation have been given in terms of peak undershoots, tie-line and frequency responses settling times, IAE, ITAE, ISE, and ITSE.

In [15], to propose a non-linear fuzzy PID-controller synchronized with a thermistor-controlled series compensator for the load frequency control problem, a brand-new modified differential evolution (MDE) method is employed. Additionally, [16] proposes a Fractional Order PID controller for load frequency management (LFM) based on Gases Brownian Motion Optimization while taking governor saturation into account [17]. Performance of the algorithm is robust to changes in parameter values. According to [18], a unique combination of Teaching Learning Based Optimization and Local Unmoral Sampling is used to produce the fuzzy PID controller scaling factors. The findings made it abundantly evident that the recommended hybrid technique can produce a better outcome than the traditional PID controllers. Additionally, [19] presents a unique hybrid Pattern Search (PS) and PSO-based fuzzy PI controller for AGC. The results of the method are comparing to those of other techniques like GA, DE, classic Ziegler Nichols (ZN), BFOA, and hybrid BFOA-PSO [20]. The proposed fuzzy PI-controller is resilient to variations in system characteristics and loading circumstances.This paper proposes a hybrid technique for LFC of modern interconnected power system. The proposed hybrid technique is combined with Sand Cat Swarm Optimization (SCSO) and Spiking Neural Network (SNN). Remaining paper is described as below: The literature review of recent work is explained in section 2. Configuration of load frequency used in power system is explained in section 3. The SCSO-SNN method and its process is clarified in section 4. The simulation and results is explained in section 5. Lastly, the conclusion is explained in section 6

2. Literature Survey

Several research works have earlier presented in the literature is depends on the Load Frequency control of modern interconnected power system utilizing several methods and features. Here, few of them are revised.

D Guha et al. [21] have explained the LFC by putting into practice a brand-new heuristic optimization technique dubbed quasi-oppositional-based JAYA (QOJAYA). The knowledge of QO-based learning was combined into the algorithm to hasten convergence and identify the most effective LFC issue solutions. In order to demonstrate effectiveness, the QOJAYA approach was independently applied to 2 area multi-unit multi-source power plant and 3 area hydro-thermal power plants. The famous PI controller's performance sufficiency and structural simplicity compel the best secondary controller design at the outset. According to A. Latif et al. [22], the variable demand and generation characteristics in modern power networks have made LFM more important. The complexity of the LFM task is increased by the incorporation of RSs into the power systems. To reduce the power mismatch of the specific power system, secondary frequency control, also known as LFM aim, was introduced to single and multi-area power systems. For single- and multi-area systems, this aids control the system frequency, and for multi-area systems, it helps plan the tie-line power exchange. Load frequency controllers were created in order to regulate and minimize the system frequency deviation. However, clever soft computing methods that take into consideration many controllers were applied to ensure the best possible power management. This study intends to give an overview of several controllers used in LFM power systems powered by traditional and renewable energy sources. N Jalali et al. [23] have suggested LFC regarded as one of the most crucial services in the function and planning of the contemporary electric power system. Due to the different structural and non-structural uncertainties in power systems, utilizing control techniques with set parameters may not output in the system performing at its best. In order to control load frequency for linked multi-area power systems in the presence of parametric uncertainties and external disturbances, this research creates a special fuzzy PID controller. The algorithm updates the model parameters and scaling factors of the output and input membership functions as well as the weights of the fuzzy PID controller rule values. The fuzzy rule weight values were determined based on the area control error (ACE) variable partitioning's transient response.

A.O. Aluko et al. [24] have to restructured power system faced significant problems in managing the many uncertainties in the output of renewable energy and load demands. With a strong UIO for dynamic state estimation and an interval type-2 FLC, this work recommends developing a novel control strategy for adaptive load frequency control of linked power systems with significant renewable energy saturation in a reorganized power system

environment. P A Gbadega and K T Akindeji [25] have suggested the frequency was a important criterion for the large-scale, multi-area power systems' dependability. The linked power system needed stability, which could only be provided by active power balance and constant frequency. It was fascinating to learn that active power balance was necessary for frequency. An LFC system must be designed to regulate power generation and the active power at the tie lines in order to increase the dependability of the power networks. In this study, controls for complicated power systems were designed using a subset of classical-control theory that was thought to be an optimum control idea by reducing a performance index depends on the system-variables. A Kazemy and M Hajatipour [26] have explained a design of LFC for multi-area power networks with linked Markovian jumps. The probability of cyber-attacks was unavoidable because the electricity system was dispersed across a wide region and therefore needed a communication network to exchange data. Denial-of-service (DoS) assault, the most frequent attack in power systems, was thus taken into consideration for the communication route. P Gaur et al. [27] have modern power system, Due to their quick charging/discharging capabilities; vehicles-to-grid (V2G) were likely to play a bigger role in contributing to ancillary services like frequency control. V2G technology may be used to manage the gap between supply and demand. In light of these considerations, this research suggests a load frequency management strategy including RES and vehicles-to-grid that can improve system-dynamics during load variations. The multi-source system including a solar-thermal power plant (STPP), a thermal unit, a gas unit, and an EV fleet in Area-1; two thermal units and an EV fleet in Area-2 and -3, respectively, was created for this.

2.1. Background of Recent Research Work

The LFC sector has effectively used a variety of controller designs and optimization approaches to enhance power systems. It was discovered that when the fuzzy PI/PID controller is employed, 2 issues arise: first, how to select the PI/PID controller's optimal gains; and second, how to pick the best design parameters for the fuzzy logic to increase its effectiveness. These 2 challenges are significant because the optimal gains of the PI/PID controller selection affect the appropriate design parameters of the fuzzy logic in one way, and in the other direction. As a result, it is necessary to determine both the fuzzy logic design settings and the PI/PID controller's optimal gains at the same time. Fuzzy logic was utilized to choose the best PI/PID increases. The use of fixed design parameters may not produce the performance of best system in real systems because of parameter uncertainty and outside disruptions. To solve this problem, this paper introduces a new fuzzy PID controller for the LFC of interconnected multi-area power systems in the face of parametric uncertainties and load disruptions.

3. Configuration of Load Frequency Used in Power System

Configuration of LFC in PV and WT is portrayed in fig 1. This paper presents a two hybrid power system. Solar and wind are the two categories. The block diagram of a hybrid renewable 2-area non-linear power system is shown in fig 1. Photovoltaic system is presented in area 1. Filter and wind energy conversion system (WECS) area 2. A 0.5 loading factor change has resulted in a 2000 MW gross active power rating for the control region. The network features a 2000 MVA complicated base power. The network parameter values are exported. The above-mentioned blocks are represented linearly as a 1st order transfer-function in the S-domain, where K denotes component's gain, T denotes time-constant of stated component, T12 denotes synchronization constant, B denotes frequency bias constant in the control region, R denotes speed factor of the governor, and suffixes g, t, and h denotes the reheated component. Additionally, the RES structure is made so that every control zone has STPP with a capability and that areas 1 and 2 each have wind power plants with capabilities of 85 MW and 50 MW, correspondingly.

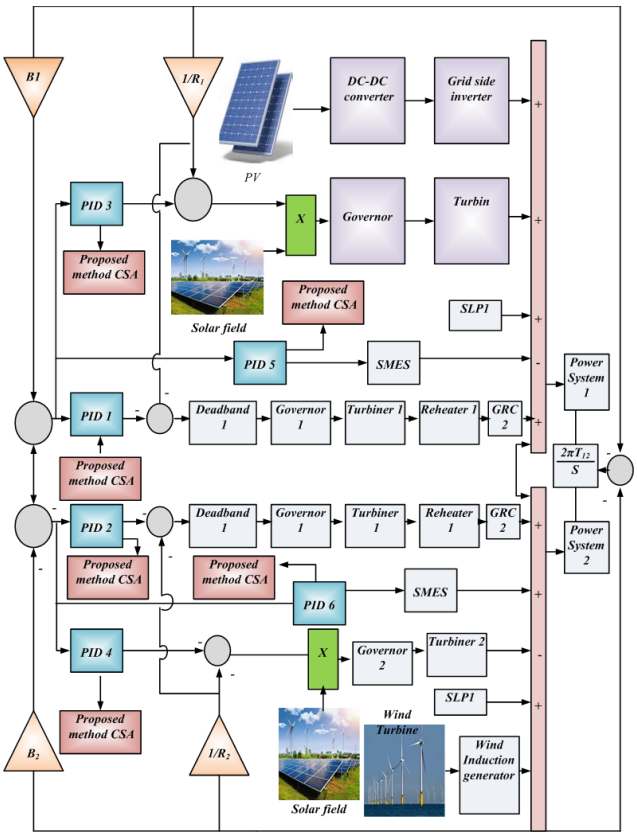

Fig. 1. Configuration of LFC in PV and WT

3.1. Modeling of Wind Power Plant

In this work, the real-time wind speed changes are included into the system model to provide a realistic simulation of the wind power plant [28]. An onshore fixed-speed wind that is in operation exported real wind fluctuations. Configuration of LFC in PV and WT is illustrated in Fig. 1 . From the fig, the wind farm is placed in area 2 and has an overall nominal capacity as 85,000 KW. One hundred wind turbines totaling 850 KW every make up the wind farm layout. The turbines employed in wind farms are Games G52/850 prototypes, and their Chirac tourism features are extensively explained. Depending on the following relationship, wind turbine transforms the input wind speed to active power. (p_t).

$$P_t = 0.125\rho\pi D^2 V_w^3 C_p(\lambda,\beta)$$

(1)

Where, the actual energy generated by the turbines signifies P_t, the amount of total Wind power is converted into useable mechanical power signifies C_p. the wind-speed in (m/s) signifies V_w, ρ as the air-density in (Kg/m3), D as the turbine-blade diameter in (m). According to the Betz limit, the value of C_P is theoretically restricted to 59.3%. The following is a mathematical representation of C_P.

$$C_\rho(\lambda,\beta) = \frac{\left(\lambda_i - 0.002\beta^2 - 5.6\right)e^{-0.17\lambda_i}}{2}$$

(2)

$$\lambda = \frac{\omega_t D}{2V_w} and \lambda_i = \frac{1800D}{1609\lambda}$$

(3)

Where λ represents the tip speed rate, ω_t signifies the turbine's rate of rotation and β the operational value of C_p is changed by putting the pitch angle management method into practice, which is used to guarantee the turbine is working at its peak output. Applying the aforementioned control technique has resulted in the wind power facility being excluded from the LFC main scheme. For the purposes of this analysis, it is anticipated that the farm's current wind turbine generators will be united into a single, tremendously powerful integrated induction generator. The integrated induction wind generator (IWG) has a 1st order-lag transfer

function. $T.F_{IWC} = \frac{K_{IWC}}{1+sT_{IWC}}$

(4)

Where, the gain of IWG signifies K_{IWC} and time-constant signifies T_{IWC}.

3.2. Modeling of PV Power Plant

Fig 3 portrays Circuit diagram of a PV model with a single diode, where the model's selection is seen to be a good balance between accuracy and model complexity [29]. The model's equations are given as follows.

$$I = I_{ph} - I_0\left[\exp\left(\frac{V+IR_s}{a}\right)-1\right] - \frac{V+IR_s}{R_{sh}}$$

(5)

Where the series resistance signifies R_s, the photocurrent signifies I_{ph}, the modified diode idealist factor signifies a, the shunt resistance signifies R_{sh} and the diode saturation current signifies I_0. According to the following relationship, the value of I_{ph} is dependent on the functioning temperature as well as solar-radiation.

$$I_{ph} = I_{ph(st)} - C_i[T - T_{st}]G$$

(6)

Here the suffix (st) represents the standard-conditions,

The operating temperature is denoted by the factor T, and the normalized solar radiation is denoted by the factor G, which is the ratio of the operating irradiation to the standard radiation. This factor describes the rate at which short circuit current changes with temperature. A photovoltaic power-station is located in area-1 for the analysis's needs. The station has a 50 MW active power rating and is made up of 250 PV panels, every with a capacity of 200 KW. The system's structure consists of 50 shunt threads, each containing 5 series-panels. Kyocera KC200GT module serves as the prototype for the PV arrays that have been put into use, and its specs are given.

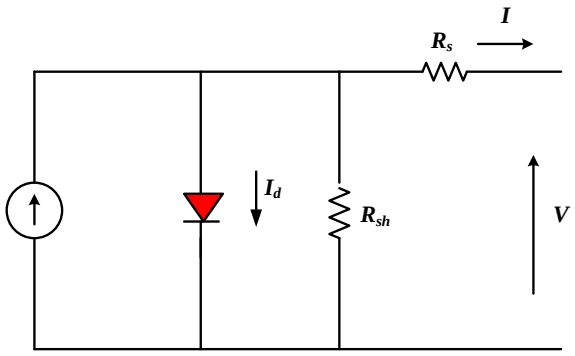

Fig. 3. Circuit diagram of a photovoltaic model with a single diode

The converter and inverter stage are the two steps that make up the PV-grid interface. The major goal of the first stage is to guarantee the PV power stations optimal power

functioning. As a result, the PV system is not a part of the LFC's main plan. Controlling the electricity flow among the photovoltaic system and grid is the inverter's main duty.

Assumed to be a 1st order lag, the transfer-function of photovoltaic-grid interface is written by below.

$$T.F_{GI} = \frac{K_{GI}}{1 + sT_{GI}} \quad (7)$$

Here, the photovoltaic-grid interface gain represents K_{GI} and its time-constant represents T_{GI} .

3.3. Modeling of PID Controller

Modeling a PID (Proportional-Integral-Derivative) controller involves determining the transfer function or mathematical representation of the controller's behavior. This transfer function defines the generation of the control output by the controller in response to variations in the error signal. A PID controller's general form is provided by:

$$C(s) = K_p + K_{i/s} + K_d * s \quad (8)$$

Here, C(s) represents transfer-function of the Proportional-Integral-Derivative controller, s represents complex frequency variable in the Laplace domain. K_i, K_d, and K_p, and are the integral, derivative gains and proportional, correspondingly.

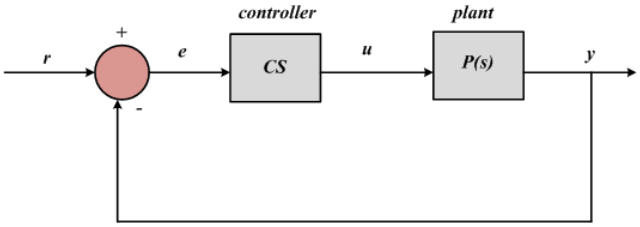

To model a PID controller, you typically start by determining the transfer function of each component (proportional, integral, and derivative) and then combine them together. To model a PID controller using process variable (PV) details, you need to consider the characteristics of the controlled process and incorporate them into the controller model. The modeling process typically involves identifying the process dynamics and determining the appropriate transfer function representation.

4. Load Frequency of Control System Using SCSO-SNN

This paper the proposes a hybrid technique is combined with the Sand Cat Swarm Optimization (SCSO), and Spiking Neural Network (SNN). The SCSO generate the control signal of the converter and the RERNN method predicts the control-signal from the SCSO technique. The detailed explanation of SCSO-SNN method is defined as below,

4.1. Sand Cat Swarm Optimization (SCSO)

Fig 4 shows the SCSO Algorithm in Exploitation VS Exploration. It is a cutting-edge approach to population-based optimization that imitates the sand cat's typical foraging and hunting behaviors [30]. These cats are expert diggers and can detect low frequencies as low as 2 kHz.

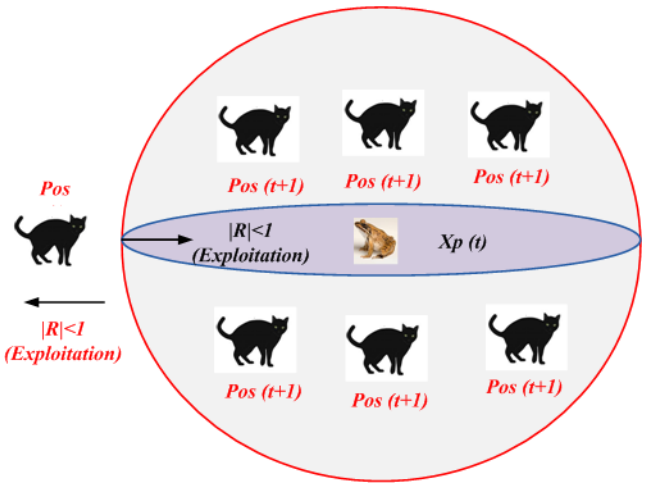

Fig. 4. SCSO Algorithm in Exploitation VS Exploration

Step 1: Initial population

Initialize the random generation parameters for the of proportional-integral is K_p and K_i . Allocate the input values as current and voltage.

Step 2: Random Generation

The input-parameters are generated at random.

$$j = \begin{bmatrix} z_{11} & z_{12} & \ldots. & z_{1d} \\ z_{21} & z_{22} & \ldots.. & z_d \\ \ldots. & & & \ldots. \\ k_{m1} & k_{m2} & \ldots.. & k_{md} \end{bmatrix} \quad (9)$$

K= population

Step 3: Fitness Assessment:

Based on the current optimal position, the initialization parameters are chosen. The fitness value of every individual should be determined.

Sand Cat $j = [z_1, z_2, \ldots z_D]$; j Ɛ population (1, k)

Fitness = (Sand Cat) = $F = Min(Error)$

(10)

$\forall zj$ is calculated for k time

Step 4: Check the Random Condition $|F| \le 1$

The adaptive value parameters fR and F provide a guarantee for exploitation and exploration. Sand-cats are instructed to attack their prey when $|F| <= 1$, else, the cats are given the responsibility of locating new potential solution in global region.

$$\vec{f}\,(T+1) = \begin{cases} \vec{f}.\overrightarrow{Pos}(T+1) - \overrightarrow{Pos}_{KD}.Cos\theta \\ \vec{f}.\overrightarrow{Pos_{bc}}(T) - rand\,(0,1) - \overrightarrow{Pos}(T).C \end{cases} \quad (11)$$

Where F as random value, T present time

5.1: Check the Search Agent Position

If $(Abs(F) <= 1)$

$$\vec{z}\,(T+1) = \{\overrightarrow{Pos}(T+1) - \overrightarrow{Pos_{fKD}}.Cos\theta.\vec{f}$$

(12)

5.2: Check the Position of Search Agent

Else $|F| <= 1$

$$\vec{f}\,(T+1) = \{\vec{f}\,\overrightarrow{Pos_{bc}}(T) - rand\,(0,1) - \overrightarrow{Pos}(T).C$$

(13)

Step 6: Termination

Verify the stopping criterion and if the optimal output is attained then process gets conclusion else go to step 3.

4.2. Spiking Neural Network (SNN)

The term SNN is used in studies to refer to any type of neural network that incorporates time as well as neuronal and synaptic states [31]. In particular, during the learning phase, the SNN algorithm may automatically update the SNN. According to diverse application information, SNN provides a optimal solution method for balancing exploitation and exploration. Neural coding is the process of using spike trains to represent data. The population, rate, and temporal encoding methods are used to encode real values. According to a temporal neural coding scheme applicable to applications for sequence modeling and forecasting, the related temporal events concealed inside the sequence are believed to be repressed.

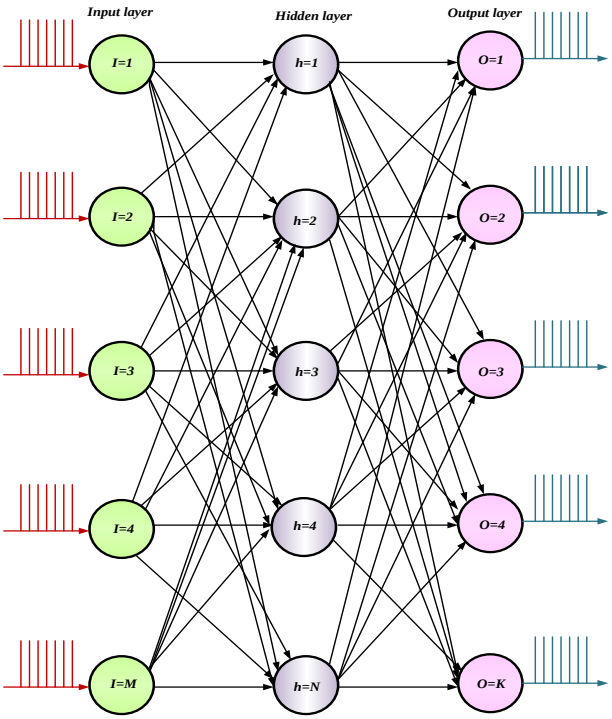

Fig. 6. Structure of Spiking Neural Network (SNN)

5. Result and Discussion

The transfer function model of investigating the power-system is created utilizing the MATLAB/SIMULINK platform. The proposed duelist algorithm's frequency-deviation, control area-error, and tie-line power are examined and simulated. In this the response examined utilizing two cases (1) Performance of SCSO-SNN Method under Constant Input and (2) Performance of SCSO-SNN Method under step changed Input. During the two situations the SCSO-SNN technique is examined and then it compares to the existing methods such as PSO, ALO and SCSO. The SCSO-SNN method is best performance than the existing technique.

Case 1: Performance of SCSO-SNN Method under Constant Input

Analysis the error of battery and photovoltaic and wind is shows in fig 6. Subplot 6(a) shows the error of battery. The error of battery is initially started from 0.57 at 0 sec. the error value is increase to reach 0.585 at 5 sec. The error is reduced to reach 0.560 at 5 sec. The remaining error value is constant 0.55 at 10 to 100 sec. Subplot 6(b) shows the error of photovoltaic. The error of PV is initially started from 0.143 at 0 sec. the error value is increase to reach to 0.148 at 5 sec. The error is reduced to reach 0.142 at 5 sec. The remaining error value is constant at 10 to 100 sec. Subplot 6(c) shows the error of wind. The error of wind is initially started from -0.18 at 0 sec. the error value is again decrease to reach to -0.182 at 5 sec. The error is increase to reach -0.183 at 52 sec. The remaining error value is constant at 10 to 100 sec. Comparison of battery error with

SCSO-SNN and existing technique is shown in fig7. Subplot 7(a) shows the proposed method battery error value is initially started from 0.57 to 0 sec, and then they increase to reach 0.585 at 1 sec. Then they value is reduced to reach 0.573 at 2sec.The battery error value is increase to 0.55 at 5sec. The remaining battery error value is constant 0.55 at 10sec to 100 sec. The proposed method battery error value is 0.573 which is higher than other existing methods like SCS, ALO and PSO methods. Comparison of PV error with proposed and existing method is shown in fig7. Subplot 7(b) shows the proposed method photovoltaic error value is initially started from 0.143 to 0 sec, and then they increase to reach 0.148 at 1 sec. Then they value is reduced to reach 0.142 at 2sec.The PV error value is increase to 0.143 at 5sec. The remain PV error value is constant 0.143 at 10sec to 100 sec. The proposed method PV error value is 0.142 which is higher than other existing methods like SCS, ALO and PSO methods. Comparison of wind error with proposed and existing method is shown in fig7. Subplot 7(c) shows the proposed method wind error value is initially started from -0.18 to 0 sec, and then they increase to reach -0.172 at 1 sec. Then they value is reduced to reach -0.185 at 2sec.The wind error value is increase to 0.184 at 5sec. The remaining wind error value is constant -0.184 at 10sec to 100 sec. The proposed method PV error value is -0.185 which is higher than other existing methods like SCS, ALO and PSO methods. Comparative of SCSO-SNN and existing methods frequency-deviation for

(a) battery, (b) PV, (c) wind is shown in fig8. Subplot 8(a) shows the proposed method frequency deviation for battery value is initially started from 0Hz to 0 sec, and then they increase to reach 10×10^{-3} Hz at 1 sec. Then they value is reduced to reach -2×10^{-3} Hz at 2sec, the frequency deviation for battery value is increase to 0Hz at 5sec.The remain frequency deviation for battery value is constant at 10sec to 100 sec. The proposed method frequency deviation for battery value is -2×10^{-3} Hz which is higher than other existing methods like SCS, ALO and PSO methods. Comparison of frequency deviation for PV with proposed and existing method is shown in fig8. Subplot 8(b) shows the proposed method frequency deviation for photovoltaic value is initially started from 0Hz to 0 sec, and then they increase to reach 1.5×10^{-3} Hz at 1 sec. Then they value is reduced to reach -0.2×10^{-3} Hz at 2sec, the frequency deviation for PV value is increase to 0Hz at 5sec.The remain frequency deviation for PV value is constant at 10sec to 100 sec. The proposed method frequency deviation for PV value is -0.2×10^{-3} Hz which is higher than other existing methods like SCS, ALO and PSO methods. Comparison of frequency deviation for wind with proposed and existing method is shown in fig8. Subplot 8(c) shows the proposed method frequency deviation for wind value is initially started from 0Hz to 0 sec, and then they decrease to reach -3×10^{-4} Hz at 1 sec. The value is increase to reach -0.2×10^{-4} Hz at 5sec.The remains frequency deviation for wind value is constant at 10sec to 100 sec. The proposed method frequency deviation for wind value is -0.2×10^{-4} Hz which is higher than other existing methods like SCS, ALO and PSO methods

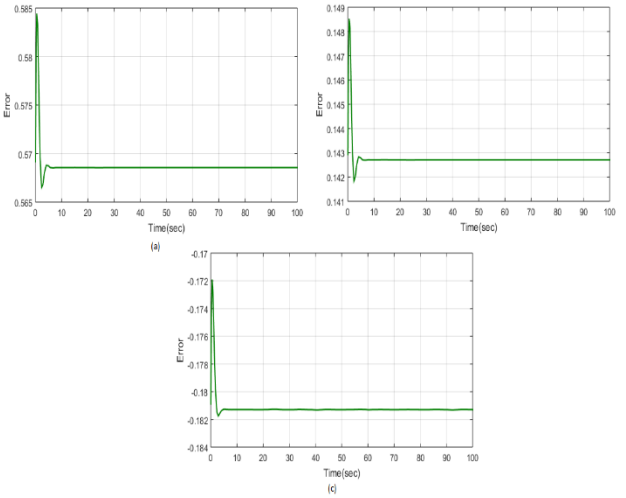

Fig. 6. Analysis the Error of (a) battery, (b) photovoltaic, (c) wind

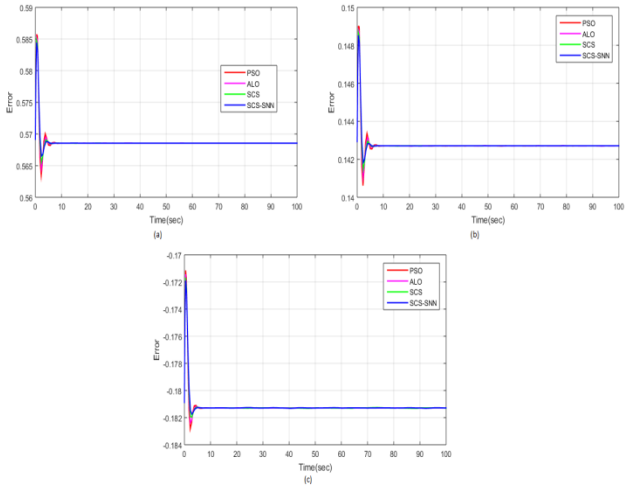

Fig 7: Comparison of SCSO-SNN and existing approaches error of
(a) battery (b) photovoltaic (c) wind.

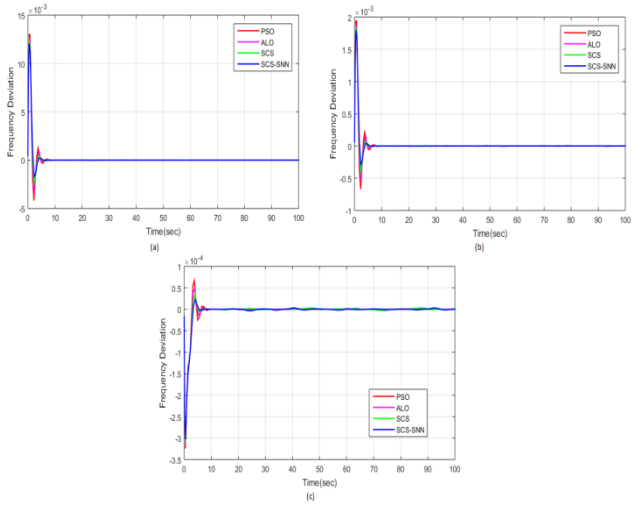

Fig 8. Comparative of SCSO-SNN and existing methods frequency-deviation for (a) battery, (b) PV, (c) wind

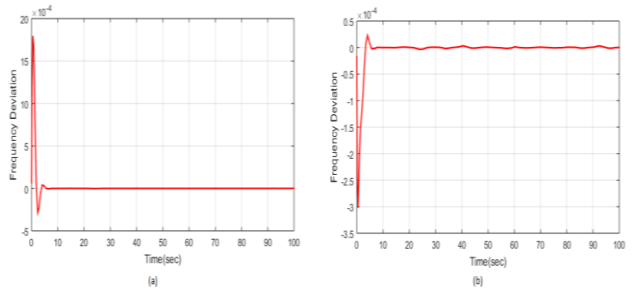

Fig. 9. Analysis the frequency deviation of (a) PV and (b) wind

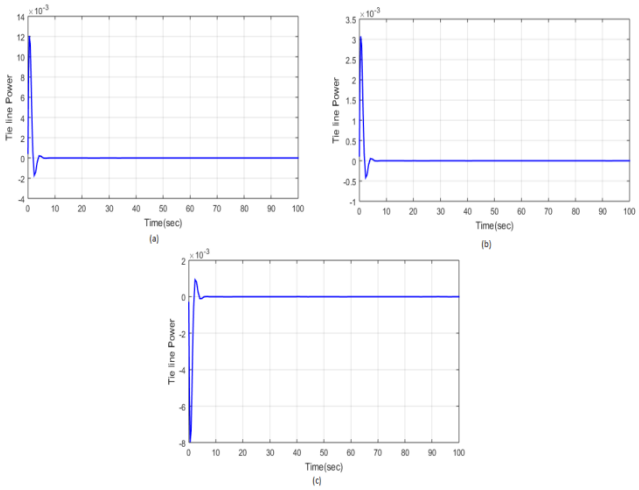

Fig 10: Analysis the Tie-line power for (a) battery, (b) photovoltaic,
(c) wind

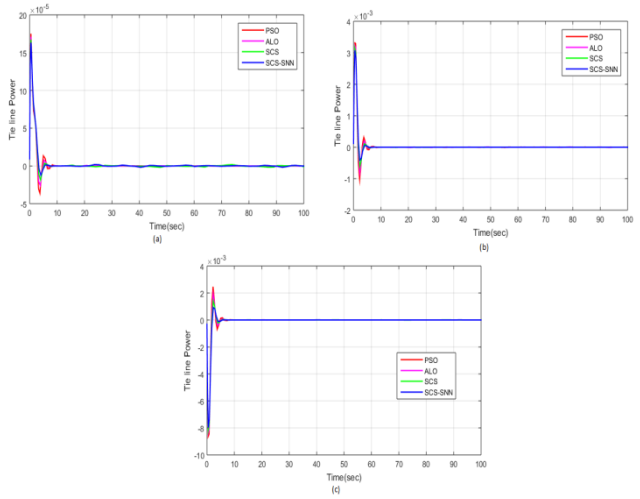

Fig. 11: Comparison of proposed and existing methods Tie line power for (a) battery (b) photovoltaic (c) wind

Fig 9 portrays analysis the frequency-deviation of PV and wind. Subplot 9(a) portrays the frequency deviation of PV. The frequency-deviation of PV is initially started from 0HZ at 0 sec. the frequency deviation of PV increase to 16 $\times 10^{-4}$ HZ at 5 sec. Then they reduced to reach -2$\times 10^{-4}$ HZ at 5 sec. The frequency deviation of PV value is constant 0HZ at 10 to 100 sec. Subplot 9(b) portrays the frequency deviation of wind. The frequency-deviation of wind is initially started from 0HZ at 0 sec. the frequency deviation of wind increase to 0.3$\times 10^{-4}$ HZ at 5 sec. The frequency deviation of wind value is constant 0HZ at 10 to 100 sec. Analysis the Tie-line power of battery and PV and wind is shows in fig 10. Subplot 10(a) shows the Tie-line power of battery. Tie-line power of battery is initially started from 0W at 0 sec then they increase to reach at 12 $\times 10^{-3}$ W at 2 sec. Tie-line power of battery is reduced to reach at -2$\times 10^{-3}$ W to 5sec. Tie-line power of battery value is constant to 0W at 55sec to 100sec.Subplot 10(b) shows the Tie-line power of PV. Tie-line power of PV is initially started from 0W at 0 sec then they increase to reach at 3$\times 10^{-3}$ W at 2sec. Tie line power of PV value is decrease to reach -0.5$\times 10^{-3}$ W at 5 sec. Tie-line power of battery value is constant to 0W at 55sec to 100sec.Subplot 10(c) shows the Tie-line power of wind. Tie-line power of wind is initially started from 0W at 0 sec, and then they decrease to reach at -8$\times 10^{-3}$ W at 2sec. Tie-line power of wind value is increase to reach 2$\times 10^{-3}$ W at 5sec. Tie line power of battery value is constant to 0W at 55sec to 100sec. Comparative of Tie-line power battery with proposed and existing method is shown in fig11. Subplot 11(a) shows the proposed method of tie line power battery value is initially started from 0W to 0 sec, and then they increase to reach 15$\times 10^{-5}$ W at 2 sec. The tie line power battery value is reduced to reach -0.2$\times 10^{-5}$ W at 5sec.The

remain Tie line power battery value is constant 0W at 55sec to 100 sec. The proposed method frequency deviation for battery value is -2×10^{-5} W which is higher than other existing methods like SCS, ALO and PSO methods. Subplot 11(b) shows the proposed method tie line power for PV value is initially started from 0W to 0 sec, and then they increase to reach 3×10^{-3}W at 1 sec. Then they value is reduced to reach -0.3×10^{-3}W at 2sec.The remain Tie line power battery value is constant 0W at 55sec to 100 sec. The proposed method tie line power for PV value is -0.3×10^{-3}W which is higher than other existing methods like SCS, ALO and PSO methods. Subplot 11(c) portrays the proposed method of tie line power wind value is initially started from 0W to 0 sec, and then they decrease to reach -8×10^{-3}W at 2sec.the value is increase to 1×10^{-3}W at 5sec.The remain tie line power wind value is constant 0W at 5sec to 100 sec. The proposed method frequency deviation for battery value is -8×10^{-3}W which is higher than other existing methods like SCS, ALO and PSO methods.

Case 2: Performance of PSCSO-SNN Method under step changed Input

Analysis the error of battery and PV and wind is shows in fig 12. Subplot 12(a) shows the error of battery. The error of battery is initially started from 0.6 at 0 sec. The error is constant at 0.6 to 50 sec. Then they error value is again increase to reach to 2.8 at 50 sec. The error is reduced to reach 2.7 at 52 sec. The remaining error value is constant at 2.7 to 100 sec. Subplot 12(b) shows the error of PV. The error of PV is initially started from 0.15 at 0 sec. The error is constant at 0.15 to 50 sec, then they error value is again increase to reach to 0.6 at 50 sec. The error is reduced to reach 0.7 at 52 sec. The remaining error value is constant at 0.7 to 100 sec. Subplot 12(c) shows the error of wind. The error of wind is initially started from -0.18 at 0 sec. The error is constant at -0.18 to 50 sec. Then they error value is again decrease to reach to -0.9 at 50 sec. The error is increase to reach -0.89 at 52 sec. The remaining error value is constant at -0.89 to 100 sec. Analysis the frequency deviation of battery and PV and wind is shows in fig 13. Subplot 13(a) portrays the frequency deviation of battery. The frequency deviation of battery is initially started from 0Hz at 0 sec then they increase to reach at 0.012 at 1 sec. the frequency deviation of battery is reduced to reach at -0.09Hz to 2sec.Then they value is constant 0Hz at 5 to 50sec. The frequency deviation of battery is again increase to reach 0.05Hz at 50sec,then they value is decrease to reach 52Hz at -0.015sec.The value is again increase to 0Hz at 55sec.The remain frequency deviation of battery value is constant at 0Hz to 100 sec. Subplot 13(b) portrays the frequency deviation of PV. The frequency deviation of PV is initially started from 0Hz at 0 sec then they increase to reach at 1.9×10^{-3} at 1sec. The frequency deviation of PV value is decrease to reach -0.9 $\times10^{-3}$Hz at 2 sec. The value is constant in 0Hz at 3sec to 50sec. The frequency deviation of PV is again increase to reach 7.5×10^{-3} at 50sec, then they value is decrease to reach 52Hz at -1.5×10^{-3}sec. The value is again increase to 0Hz at 55sec.The remain frequency deviation of PV value is constant at 0Hz to 100 sec. Subplot 13(c) portrays the frequency deviation of wind. The frequency deviation of wind is initially started from 0Hz at 0 sec then they decrease to reach at -3×10^{-4} Hz at 1sec.The frequency deviation of wind value is increase to reach -0.1×10^{-4} Hz at 5sec. The value is constant in 0Hz at 5sec to 50sec. The frequency deviation of wind is again decrease to reach -0.12×10^{-4} Hz at 50sec,then they value is increase to1 $\times10^{-4}$ at 55sec.The value is again decrease to 0Hz at 55sec.The remain frequency deviation of wind value is constant to 0Hz at 55sec to 100 sec. Comparative of frequency deviation for battery with SCSO-SNN and existing method is shown in fig14. Subplot 14(a) shows the proposed method frequency deviation for battery value is initially started from 0Hz to 0 sec, and then they increase to reach 0.012Hz at 1 sec. Then they value is reduced to reach -0.019Hz at 2sec. The frequency deviation for battery is constant 0Hz at 5 to 50sec, then they value is increase to 0.05Hz at 50sec.The frequency deviation for battery is reduced to reach -0.012Hz at 52sec, then they value is again increase to 0Hz at 55sec. The remaining frequency deviation for battery value is constant at 55sec to 100 sec. The proposed method frequency deviation for battery value is -0.019Hz which is higher than other existing methods like SCS, ALO and PSO methods. Comparison of frequency deviation for PV with proposed and existing method is shown in fig14. Subplot 14(b) shows the proposed method frequency deviation for PV value is initially started from 0Hz to 0 sec, and then they increase to reach 2×10^{-3}Hz at 1 sec. Then they value is reduced to reach -1×10^{-3}Hz at 2sec. The frequency deviation for PV is constant 0Hz at 5 to 50sec, then they value is increase to 7×10^{-3}Hz at 50sec.The frequency deviation for PV is reduced to reach -1×10^{-3}Hz at 52sec, then they value is again increase to 0Hz at 55sec. The remaining frequency deviation for PV value is constant at 55sec to 100 sec. The proposed method frequency deviation for PV value is -1×10^{-3}Hz which is higher than other existing methods like SCS, ALO and PSO methods. Comparison of frequency deviation for wind with proposed and existing method is shown in fig 14. Subplot 14(c) shows the proposed method frequency deviation for wind

value is initially started from -3×10^{-4} Hz to 0 sec, and then they increase to reach 0Hz at 5 sec. The frequency deviation for wind is constant 0Hz at 5 to 50sec, Then they value is reduced to reach -12×10^{-4} Hz at 50sec.the value is increase to 0.5×10^{-4} Hz at 52sec.The frequency deviation for wind is reduced to reach 0Hz at 55sec.The remain frequency deviation for wind value is constant at 55sec to 100 sec. The proposed method frequency deviation for PV value is 0.5×10^{-4} Hz which is higher than other existing methods like SCS, ALO and PSO methods.

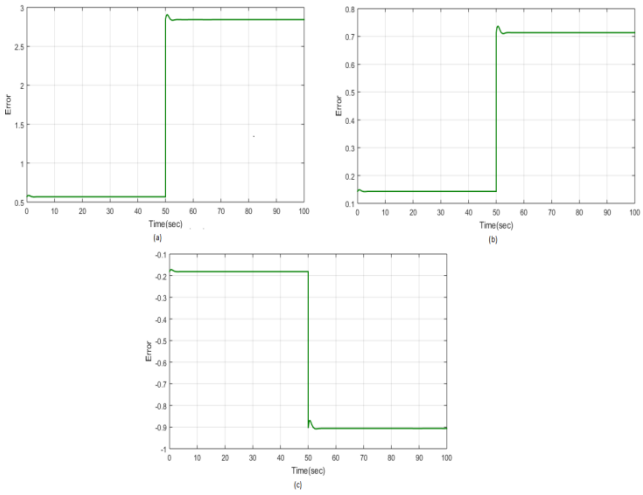

Fig 12: Analysis the Error of (a) battery (b) photovoltaic (c) wind

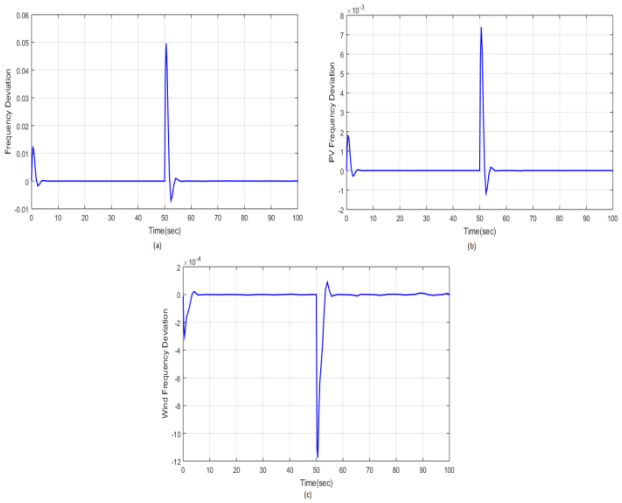

Fig 13: Analysis the frequency deviation for (a) battery and (b) photovoltaic (c) wind

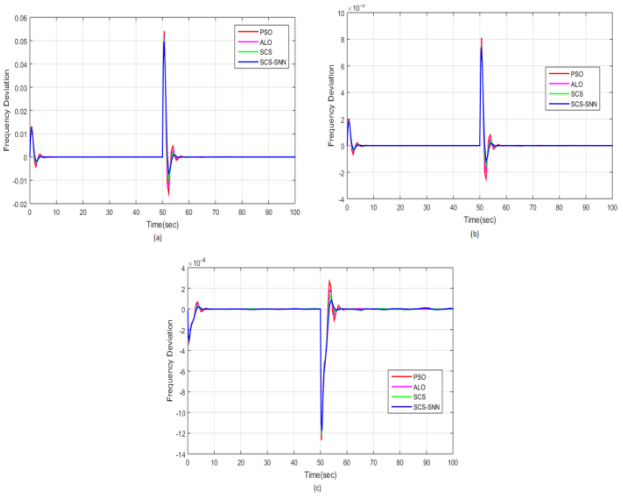

Fig 14: Comparative of SCSO-SNN and existing methods frequency deviation for (a) battery, (b) PV, (c)wind

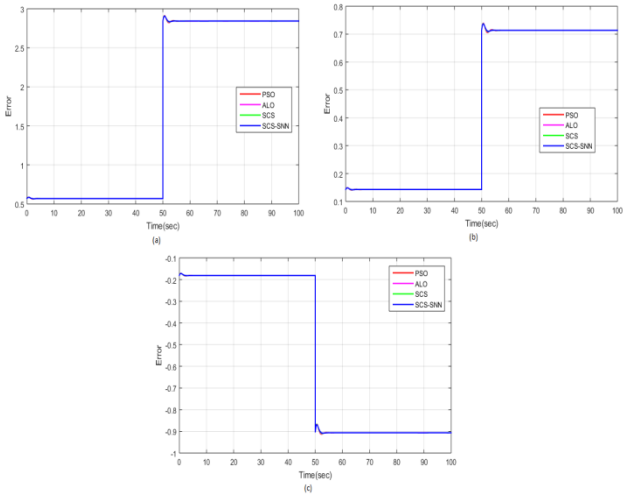

Fig 15: Comparison of proposed and existing methods error of (a) battery, (b) Photovoltaic,(c) wind.

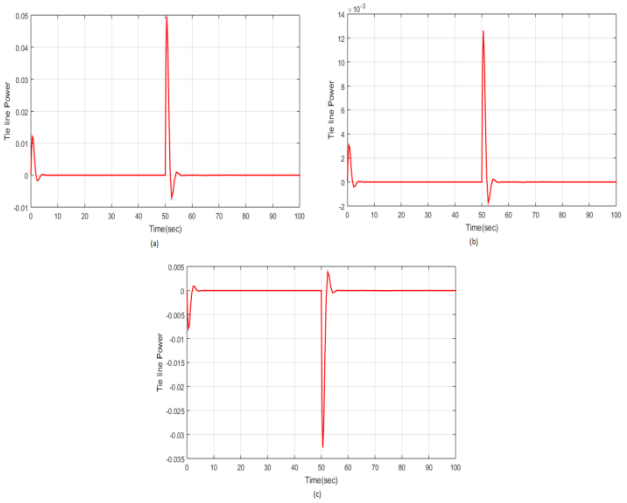

Fig 16: Analysis the Tie line power for (a) battery, (b) Photovoltaic, (c) wind

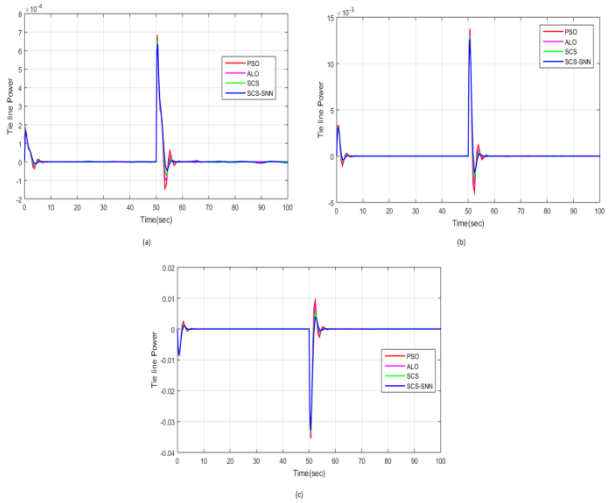

Fig 17: Comparison of proposed and existing methods Tie line power for (a) Battery, (b) photovoltaic, (c) wind

Comparison of battery error with proposed and existing method is shown in fig15. Subplot 15(a) shows the proposed method of battery error value is initially started from 0.5 to 0 sec, and then they value is constant 0 to 50sec.The battery error value is increase to reach 2.8 at 50 sec. The value is reduced to reach 2.6 at 52sec.The remain Error value is constant at 55sec to 100 sec. the proposed method error value is lesser than existing method. Subplot 15(b) shows the proposed method of photovoltaic error value is initially started from 0.15 to 0 sec, and then they value is constant 0 to 50sec.The PV error value is increase to reach 0.74 at 50 sec. The value is reduced to reach 0.7 at 52sec.The remain Error value is constant at 55sec to 100 sec. the proposed method error value is lesser than existing method. Subplot 15(c) shows the proposed method of wind error value is initially started from -0.19 to 0 sec, and then they value is constant 0 to 50sec.The wind error value is decrease to reach -0.9 at 50 sec. Then they value increase to reach -0.89 at 52sec.The remain wind error value is constant at 55sec to 100 sec the proposed method error value is lesser than existing method. Analysis the Tie line power of battery and PV and wind is shows in fig 16. Subplot 16(a) shows the Tie-line power of battery. Tie line power of battery is initially started from 0W at 0 sec then they increase to reach at 0.012W at 1 sec. Tie line power of battery is reduced to reach at -0.09W to 2sec.Then they value is constant 0W to 50sec. The Tie line power of battery is again increase to reach 0.05W at 50sec,then they value is decrease to reach 52W at -0.09sec.The value is again increase to 0W at 55sec.The remain Tie line power of battery value is constant to 0W at 55 to 100 sec. Subplot 16(b) shows Tie line power of photovoltaic. Tie line power of PV is initially started from 0W at 0 sec then they increase to reach at 3×10^{-3}W at 1sec. Tie line power of PV value is decrease to reach -0.9$\times10^{-3}$W at 2 sec. The value is constant in 0W at 5sec to 50sec. The Tie line power of PV is again increase to reach 13×10^{-3} W at 50sec, then they value is decrease to reach 52W at -2 $\times10^{-3}$sec. The value is again increase to 0W at 55sec.The remain Tie line power of PV value is constant to 0W at 55 to 100 sec. Subplot 16(c) shows the Tie line power of wind. Tie line power of wind is initially started from 0W at 0 sec then they decrease to reach at -0.008W at 1sec.The Tie line power of wind value is increase to reach 0.002W at 5sec. The value is constant in 0W at 5sec to 50sec. Tie line power of wind is again decrease to reach -0.030W at 50sec, then they value is increase to 0.004W at 55sec.The value is again decrease to 0W at 55sec.The remain Tie line power of wind value is constant to 0W at 55sec to 100 sec. Fig 17 portrays comparison of Tie line power battery with proposed and existing method. Subplot 17(a) shows the proposed method of tie line power battery value is initially started from 0W to 0 sec, and then they increase to reach 2 $\times10^{-4}$ W at 1 sec. Then they value is reduced to reach -0.09$\times10^{-4}$ W at 5sec. The tie line power battery is constant 0W at 5 to 50sec, then they value is increase to 6.5$\times10^{-4}$ W at 50sec.The tie line power battery is reduced to reach -0.06$\times10^{-4}$ W at 52sec, then they value is again increase to 0W at 55sec. The remain Tie line power battery value is constant 0W at 55sec to 100 sec. The proposed method frequency deviation for battery value is -0.06 $\times10^{-4}$ W which is higher than other existing methods like SCS, ALO and PSO methods. Subplot 17(b) shows the proposed method tie line power for photovoltaic value is initially started from 0W to 0 sec, and then they increase to reach 4$\times10^{-3}$W at 1 sec. Then they value is reduced to reach -1$\times10^{-3}$W at 2sec. The tie line power for PV is constant 0W at 5 to 50sec, then they value is increase to 12 $\times10^{-3}$W at 50sec.The tie line power for PV is reduced to reach -2$\times10^{-3}$W at 52sec, then they value is again increase to 0W at 55sec. The remaining tie line power for PV value is constant 0W at 55sec to 100 sec. The proposed method tie line power for PV value is -2$\times10^{-3}$W which is higher than other existing methods like SCS, ALO and PSO methods. Subplot 17(c) shows the proposed method of tie line power wind value is initially started from -0.01W to 0 sec, and then they increase to reach 0W at 5 sec. The tie line power wind is constant 0W at 5 to 50sec, Then they value is reduced to reach -0.03W at 50sec.the value is increase to 0.005W at 52sec.The tie line power wind is reduced to reach 0Hz at 55sec.The remain tie line power wind value is constant 0W at 55sec to 100 sec. The proposed method tie line power for PV value is 0.005 which is higher than other existing methods like SCS, ALO and PSO methods.

6. Conclusion

This study suggests hybrid SCSO-SNN approach for LFC of Modern interconnected Power System utilizing SCSO-SNN approach. The SCSO-SNN technique demonstrates the 2-area power system like solar and wind system. The control strategy offers a stronger control than the available techniques while maintaining effective transient performance. The SCSO-SNN technique is evaluated in the MATLAB/Simulink platform and contrasted with different other methods already in use. Numerous situations, including optimal and random scheduling and an elaborate SCSO algorithm, are used to evaluate the suggested technique. From the result, it is concluded that the SCSO-SNN technique-based error is less compared to existing techniques. The goal of the SCSO-SNN technique is to control error and increase the efficiency. The outcomes also demonstrate that the SCSO-SNN technique performs notably best than the other optimization techniques. The simulation result of SCSO-SNN technique is validated under two cases, such as SCSO-SNN technique performance under constant input and performance of SCSO-SNN technique under constant input. The proposed method is battery error value is 2.7%, which is lower value compare with other existing methods.

Reference

[1] Tarkeshwar and V. Mukherjee, "A novel quasi-oppositional harmony search algorithm and Fuzzy Logic Controller for frequency stabilization of an isolated hybrid power system," International Journal of Electrical Power & Energy Systems, vol. 66, pp. 247–261, 2015. doi:10.1016/j.ijepes.2014.10.050

[2] A. Ghasemi-Marzbali, "Multi-area multi-source automatic generation control in Deregulated Power System," Energy, vol. 201, p. 117667, 2020. doi:10.1016/j.energy.2020.117667

[3] Review for "Load frequency control of a M ulti-source multi-area thermal system including biogas–solar thermal along with pumped Hydro Energy Storage System using MBA -optimized 3DOF-TIDN controller," 2021. doi:10.1002/2050-7038.13165/v2/review2

[4] Yanamadni, V. R. ., Seetha, J. ., Kumar, T. S. ., Kannaiah, S. K. ., J, B. ., & Brahmaiah, M. . (2023). Computer-Aided Detection of Skin Cancer Detection from Lesion Images via Deep-Learning Techniques. International Journal on Recent and Innovation Trends in Computing and Communication, 11(2s), 293–302. https://doi.org/10.17762/ijritcc.v11i2s.6158

[5] R. K. Khadanga, A. Kumar, and S. Panda, "A modified grey wolf optimization with cuckoo search algorithm for Load Frequency Controller design of Hybrid Power System," Applied Soft Computing, vol. 124, p. 109011, 2022. doi:10.1016/j.asoc.2022.109011

[6] R. Aljendy, Review for "bio-inspired hybrid BFOA-PSO algorithm-based Reactive Power Controller in a standalone wind-diesel power system," 2020. doi:10.1002/2050-7038.12778/v1/review2

[7] A. D. Rosaline and S. Ushakumari, "Robust loop-shaping controller for load frequency control of an uncertain deregulated power system," Journal of The Institution of Engineers (India): Series B, vol. 100, no. 4, pp. 357–369, 2019. doi:10.1007/s40031-019-00376-1

[8] S. Mishra, "Optimal tuning of 3DOF-pid and 2DOF-PID controller for Load Frequency Control," Journal of Advanced Research in Dynamical and Control Systems, vol. 24, no. 4, pp. 61–68, 2020. doi:10.5373/jardcs/v12i4/20201418

[9] H. Yadav and D. K. Sambariya, "Load frequency control for multi-area power system using Fuzzy Logic Controller," 2019 International Conference on Communication and Electronics Systems (ICCES), 2019. doi:10.1109/icces45898.2019.9002205

[10] A. Bouaddi, R. Rabeh, and M. Ferfra, "Load frequency control of autonomous microgrid system using hybrid fuzzy logic GWO-CS pi controller," 2021 9th International Conference on Systems and Control (ICSC), 2021. doi:10.1109/icsc50472.2021.9666683

[11] H. Abadlia and R. Toufouti, "Fuzzy logic based MPPT control of an isolated hybrid PV-wind-battery energy system," Digital Technologies and Applications, pp. 1745–1755, 2021. doi:10.1007/978-3-030-73882-2_158

[12] S. Chatterjee, C. K. Shiva, and V. Mukherjee, "Automatic generation control of multi-area hydro power system using moth flame optimization technique," 2019 3rd International Conference on Recent Developments in Control, Automation & Power Engineering (RDCAPE), 2019. doi:10.1109/rdcape47089.2019.8979090

[13] R. El-Sehiemy, A. Shaheen, A. Ginidi, and S. F. Al-Gahtani, "Proportional-integral-derivative controller based-artificial rabbits algorithm for load frequency control in Multi-Area Power Systems," Fractal and Fractional, vol. 7, no. 1, p. 97, 2023. doi:10.3390/fractalfract7010097

[14] H. Yadav and D. K. Sambariya, "Load frequency control for multi-area power system using Fuzzy Logic Controller," 2019 International Conference on Communication and Electronics Systems (ICCES), 2019. doi:10.1109/icces45898.2019.9002205

[15] N. K. Gupta, M. K. Kar, and A. K. Singh, "Design of a 2-DOF-PID controller using an improved sine–cosine algorithm for load frequency control of a three-area system with nonlinearities," Protection and Control of Modern Power Systems, vol. 7, no. 1, 2022. doi:10.1186/s41601-022-00255-w

[16] "Model predictive control for load frequency stabilizer," ERJ. Engineering Research Journal, vol. 42, no. 4, pp. 255–260, 2019. doi:10.21608/erjm.2019.66248

[17] Y. V. Hote and N. S. Raut, "PID controller design based on IMC using model order reduction and Modern Control Approach: Application to single area load frequency control problem," 2020 IEEE 16th International Conference on Control & Automation (ICCA), 2020. doi:10.1109/icca51439.2020.9264425

[18] S. Zhang, Z. Liu, H. Zhang, and J. Wang, "Distributed adaptive protocols design based load frequency control for multi-area interconnected power system," 2021 40th Chinese Control Conference (CCC), 2021. doi:10.23919/ccc52363.2021.9549664

[19] "A robust cascaded controller for load frequency control in renewable energy integrated microgrid containing PEV," International Journal of Renewable Energy Research, no. V13i1, 2023. doi:10.20508/ijrer.v13i1.13234.g8697

[20] M. Barakat, "Novel chaos game optimization tuned-fractional-order PID fractional-order Pi Controller for load–frequency control of interconnected power systems," Protection and Control of Modern Power Systems, vol. 7, no. 1, 2022. doi:10.1186/s41601-022-00238-x

[21] S. J. Et.al, "Gravitational search algorithm based automatic load frequency control for multi-area interconnected power system," Turkish Journal of Computer and Mathematics Education (TURCOMAT), vol. 12, no. 3, pp. 4548–4568, 2021doi:10.17762/turcomat.v12i3.1845

[22] B. Vedik, R. Kumar, R. Deshmukh, S. Verma, and C. K. Shiva, "Renewable energy-based load frequency stabilization of interconnected power systems using quasi-oppositional dragonfly algorithm," Journal of Control, Automation and Electrical Systems, vol. 32, no. 1, pp. 227–243, 2020. doi:10.1007/s40313-020-00643-3

[23] A. Latif, S. M. S. Hussain, D. C. Das, and T. S. Ustun, "State-of-the-art of controllers and soft computing techniques for regulated load frequency management of single/multi-area traditional and renewable energy based Power Systems," Applied Energy, vol. 266, p. 114858, 2020. doi:10.1016/j.apenergy.2020.114858

[24] N. Jalali, H. Razmi, and H. Doagou-Mojarrad, "Optimized fuzzy self-tuning PID controller design based on tribe-de optimization algorithm and rule weight adjustment method for load frequency control of interconnected multi-area power systems," Applied Soft Computing, vol. 93, p. 106424, 2020. doi:10.1016/j.asoc.2020.106424

[25] Mr. Dharmesh Dhabliya. (2012). Intelligent Banal type INS based Wassily chair (INSW). International Journal of New Practices in Management and Engineering, 1(01), 01 - 08. Retrieved from http://ijnpme.org/index.php/IJNPME/article/view/2

[26] M. Yang, C. Wang, Z. Liu, and S. He, "An eid load frequency control method for two-area interconnected power system with photovoltaic generation," 2021 33rd Chinese Control and Decision Conference (CCDC), 2021. doi:10.1109/ccdc52312.2021.9601590

[27] P. A. Gbadega and K. T. Akindeji, "Linear quadratic regulator technique for optimal load frequency controller design of Interconnected Linear Power Systems," 2020 IEEE PES/IAS PowerAfrica, 2020. doi:10.1109/powerafrica49420.2020.9219887

[28] P. Gaur, N. Soren, and D. Bhowmik, "Load frequency control of hybrid power system incorporating vehicle-to-grid technology considering AC transmission links," Journal of Electrical Engineering & Technology, vol. 15, no. 1, pp. 381–391, 2019. doi:10.1007/s42835-019-00134-9

[29] Q. Gao, Z. Du, Y. Song, and Y. Ji, "Periodic event-triggered resilient control for Multiarea interconnected power systems under denial-of-service attacks," 2022 IEEE International Conference on Mechatronics and Automation (ICMA), 2022. doi:10.1109/icma54519.2022.9856389

[30] M. A. Sobhy, A. Y. Abdelaziz, H. M. Hasanien, and M. Ezzat, "Marine predators algorithm for load frequency control of modern interconnected power systems including renewable energy sources and Energy Storage Units," Ain Shams Engineering Journal, vol. 12, no. 4, pp. 3843–3857, 2021. doi:10.1016/j.asej.2021.04.031

[31] A. Kirsten Vidal de Oliveira, M. Aghaei, and R. Rüther, “Aerial infrared thermography for low-cost and fast fault detection in utility-scale PV power plants,” Solar Energy, vol. 211, pp. 712–724, 2020. doi:10.1016/j.solener.2020.09.066

[32] A. Seyyedabbasi and F. Kiani, "Sand Cat swarm optimization: a nature-inspired algorithm to solve global optimization problems", Engineering with Computers, 2022. Available: 10.1007/s00366-022-01604-x [Accessed 16 September 2022].

[33] C. Liu, W. Shen, L. Zhang, Y. Du, and Z. Yuan, “Spike neural network learning algorithm based on an evolutionary membrane algorithm,” IEEE Access, vol. 9, pp. 17071–17082, 2021.